Biomass Conversion and Biorefinery
https://doi.org/10.1007/s13399-022-02327-1

ORIGINAL ARTICLE

The use of biochar-NH_2 produced from watermelon peels as a natural adsorbent for the removal of Cu(II) ion from water

Mohamed A. El-Nemr[1] · Uyiosa O. Aigbe[2] · Mohamed A. Hassaan[3] · Kingsley E. Ukhurebor[4] · Safaa Ragab[3] · Robert B. Onyancha[5] · Otolorin A. Osibote[2] · Ahmed El Nemr[3]

Received: 16 November 2021 / Revised: 6 January 2022 / Accepted: 9 January 2022

Abstract

While various techniques have been explored for the sequestration of heavy metals such as copper from industrial effluent, there is enormous research on the use of biosorbents created from bio-waste in the environment for the confiscation of Cu(II) ion owing to their low cost and green nature. In this study, a biochar-NH_2 biosorbent synthesized from watermelon peels was explored for the elimination of Cu(II) ion from water-soluble solutions. The synthesized biochar-NH_2 was further characterized using FTIR, BET, and SEM coupled with EDX to ascertain the present functional groups, the surface area, morphology, and elementary composition of the biosorbent. The determined biochar-NH_2 BET-specific surface area and the total pore volume were 12.26 m^2/g and 0.012 cm^3/g. The differential thermal analysis (DTA) of the WWP and biochar-NH_2 samples showed six peaks at flow temperatures of 769, 178, 251, 292, 426, and 872 °C, and two distinct degradation peaks at flow temperatures of 767 and 477 °C. The sequestration of Cu(II) was noted in this study to be dependent on the pH, with the best possible confiscation of Cu(II) ion noticed at pH 5.6. The process of Cu(II) adsorption to the biosorbent was perfectly defined utilizing the Langmuir (LGR) and pseudo-second-order (PSO) models with correlation coefficient (R^2) values of 0.944 and < 0.99. It is implicit that the sorption process consists of a chemisorption process in rate-limiting stages. The determined sorption capacity estimated from the Langmuir isotherm model was determined to be 140.85 mg/g and when the sorption capacity of biochar-NH_2 was compared to other biosorbents employed for the sequestration of Cu(II) ion from water-soluble solutions, the biochar-NH_2 biosorbent was found to be an effective biosorbent for Cu(II) elimination. Additionally, it was found that the biosorbent can be regenerated up to six regeneration cycles for the confiscation of Cu(II) ion. In conclusion, it was discovered in this study that the synthesized biosorbent was a cost-effective adsorbent with a high adsorption efficacy for Cu(II) removal.

Keywords Aquatic environment · Biochar-NH_2 · Copper removal · Water treatment · Pollution · Watermelon peels

✉ Ahmed El Nemr
ahmedmoustafaelnemr@yahoo.com;
ahmed.m.elnemr@gmail.com

Mohamed A. El-Nemr
mohamedelnemr1992@yahoo.com

Uyiosa O. Aigbe
uyi4we@gmail.com

Mohamed A. Hassaan
mhss95@mail.com

Kingsley E. Ukhurebor
ukeghonghon@gmail.com

Safaa Ragab
safaa_ragab65@yahoo.com

Robert B. Onyancha
08muma@gmail.com

Otolorin A. Osibote
osibotea@cput.ac.za

[1] Department of Chemical Engineering, Faculty of Engineering, Minia University, Minia, Egypt

[2] Department of Mathematics and Physics, Faculty of Applied Sciences, Cape Peninsula University of Technology, Cape Town, South Africa

[3] Environment Division, National Institute of Oceanography and Fisheries (NIOF), Kayet Bey, Elanfoushy, Alexandria, Egypt

[4] Department of Physics, Faculty of Science, Edo State University Uzairue, Uzairue, Edo State, Nigeria

[5] Department of Technical and Applied Physics, School of Physics and Earth Sciences Technology, Technical University of Kenya, Nairobi, Kenya

Published online: 17 January 2022

1 Introduction

Environmental effluences ensuing from heavy metals (HMs), wastewater (WW), and other toxic substances are now on the rise owing to the continuous evolution of industrial activities and the enormous rise in the human population [1–5]. Globally, these rising environmental effluences especially through HMs, WW, and other toxic substances from industrial activities are instigating critical environmental, climatic, and health complications to humanity and the entire ecosystems [6–13]. Reportedly, some of the main sources of these environmental effluences comprise the emissions from industries (both the organic and inorganic), waste furnaces, automobiles exhaust, and the utilization of agricultural alterations (for example, the use of sludge, pesticides, herbicides, fertilizers, and other agricultural amenities) [14, 15].

As reported by Phuengphai et al. [14], the extent of WW effluences depends on the duration and the action that contributes to the cause of the effluences on the contaminated locations. It is therefore significant to eliminate toxic HMs, WW, and other toxic substances from contaminated locations to manage harmful consequences and limit the dispersion and discharge to neighboring agricultural land and groundwater for agricultural and environmental sustainability and safety (AESS). Industries all over the world especially those included in the production of plastics, semiconductor technology, batteries, electronics, microelectronics, paints, automobiles, and inks use HMs during their manufacturing processes and convey other toxic substances to the environment in one form or the other, unavoidably contaminating water sources thereby instigating water and other environmental effluences [16]. Hence, industries are supposed to contribute significantly to the remediation processes as well as the development and advancement of the economy and society at large for AESS.

These HMs are harmful to living creatures and are now a global and rising issue that has become evident in water contamination [17, 18]. Sustaining a safe extent of HMs in water is critical due to their harmfulness and oncogenicity which are reportedly causing critical impairment to individual health and the environment. Most of the water effluences are arsenic (As), chromium (Cr), cadmium (Cd), copper (Cu), iron (Fe), lead (Pb), mercury (Hg), nickel (Ni), and zinc (Zn), which are a group of inert chemicals introduced into water sources through the untreated toxic substances (wastes) mostly from industrial activities from the fertilizer, mining, paper, plating, tanneries, wood, refining, and other industries. Reportedly, there are at the moment increasingly critical threats to human health and the environment due to the non-biodegradable nature of HMs (unlike the contaminants from organic sources) as well as the difficulties in avoiding the presence of these HMs in WW owing to the activities of industries such as smelting, mining, refining, metallurgy, and surface finishing [3, 4]. Moreover, these HMs find their way into the food chain through untreated toxic substances (WW) and this, in turn, is causing great harm and threat to both terrestrial and aquatic living organisms [3, 4].

Cu is one of the first ever extracted used metals which has continuously and extensively being used in numerous sectors and presently being utilized for various domestic, industrial, and high-technology applications among other HMs [19]. Brass manufacture, plating, electroplating, mining and smelting, petroleum refining, and in Cu-based agrochemical syntheses are just a few of the sectors that use it. Cu(II) effluents from these enterprises are released into the ecosystem in various amounts, resulting in harmful waste. It ends up posing a threat to marine life, animals, plants, and individual health. According to WHO, BIS, and USEPA, the permissible acceptable levels of Cu(II) ion in drinking water are 2.00 $mg{\cdot}L^{-1}$, 1.50 $mg{\cdot}L^{-1}$, and 1.30 $mg{\cdot}L^{-1}$, respectively [14, 16].

Consequently, several technologies have been reported and established by various researchers on the control, recovery, and confiscation of HMs vis-à-vis WW from the environment such as biosorption [20–24], chemical precipitation [25], flotation [26], electrolytic recovery [27], adsorption of HMs [27], activated carbon adsorption [28], and membrane separation [27]. Among these researches is the adsorption process which has been extensively considered as a means for solving WW problems for several industries [14, 29].

Agrarian unused biosorbents mostly employed in the biosorption investigations are vast, low cost, and non-harmful materials, which are exclusively selected for HMs and are effortlessly disposed of by burning. These agrarian by-products as a sum surpass 3.20×10^{11} kg/year and most of these by-products are considered to be low-value products [30]. At the moment, several researchers are now exploring low-cost (affordable) adsorbents with exceptional metal-binding proficiencies for the recovery and treatment of WW [9, 14, 31]. Similarly, it has been reported that several agricultural and forestry by-products such as peelings of fruits, compost, and plant leaves are now been extensively employed for the recovery and treatment of WW vis-à-vis HMs [9, 14, 32]. The flora cells primarily consist of cellulose, lignin, and tannin which have great potentialities in absorbing the ions of HMs [33–36].

Nevertheless, this present study will concentrate on the confiscation and adsorption potentialities of Cu from solutions (water), which like every other HMs are mostly from industrial activities. Excess of Cu in the blood structure could produce reactive oxygen types and impairment of the DNA, lipids, and protein in addition to affecting some

vital organs in the human system such as kidney, liver, and pancreas [16]. As reported by Manzoor et al. [37], Cu also affects the aquatic environment. They destroy some vital organs (such as the gills, liver, and kidneys) and systems (such as the nervous system) of aquatic animals as well as the modification of their sexual life. However, there are some reported studies on the adsorption potentialities in absorbing Cu(II) ion from aqueous solutions employing some natural adsorbents [14], such as pomelo peels [38], pomegranate peels [10], orange peels [39, 40], grapefruit peels [41, 42], red alga *Pterocladia capillacea* [20], pea peels *Pisum sativum* [43], bio-nanocomposite [44, 45], and even watermelon peels (WMPs) [16] as in the case of this present study. Albeit, existing publications available in various indexed journals on the study of the adsorption potentialities in removing Cu(II) ion from water (solutions) utilizing WMP as a natural adsorbent are limited. Hence, this present study attempted to further reconsider and re-explore the potentialities of using WMP as a natural adsorbent for the confiscation of Cu(II) ion. The rationale for the consideration of WMP for this study was to establish the use of biochar-NH_2 prepared from WMP using the dehydration method as a natural biosorbent for the confiscation of Cu(II) ion, which is the first of its kind. Furthermore, the experimental, characterization, and morphological studies were considered and reported.

2 Materials and methods

2.1 Materials

WMPs were obtained from a resident market in Alexandria and utilized as an unprocessed material to make biochar, which was then used to make the adsorbent. Sigma Aldrich (USA) provided the sulfuric acid (H_2SO_4, assay 99%). Copper sulphate pentahydrate ($CuSO_4{\cdot}5H_2O$) obtained from Sigma Aldrich, USA, was used to make the Cu(II) standard stock. Loba Chemie in India provided the sodium salt of diethyldithiocarbamate. The El-Naser Company in Alexandria, Egypt, provided a 25% NH_4OH solution. A "digital spectrophotometer (Analytic Jena (SPEKOL1300 UV/Visible spectrophotometer))" with matching glass cells of a 1 cm optical path, a shaker (JSOS-500), Koria, and a pH meter JENCO (6173) were employed to determine the equilibrium concentration Cu(II) ion after every batch experiments carried out, agitate mixture of Cu(II) solution and biosorbent used in the batch experiments, and adjust solution pH.

2.2 Biochar-NH_2 preparation

WMPs were carefully washed with tap water to eliminate dust and then dried for 48 h at 105 °C before milling and crushing. After boiling 200 g of crushed WMP for 2 h in an 800 mL solution of 50% H_2SO_4, the samples were filtered and washed with distilled water until the washing solution pH became neutral, followed by ethanol washing. The resulting biochar was dried at 70 °C and weighed. Biochar was made by boiling it in a refluxing system with 25% NH_4OH (200 mL), filtering it, and then washing it with distilled water and ethanol. Finally, the produced biochar was dried for 24 h at 70 °C and was labelled as biochar-NH_2.

2.3 Biochar-NH_2 characterization

Using nitrogen adsorption at 77 K, the energy constant (C), the monolayer volume (V_m) (cm^3 (STP) g^{-1}), the surface area (S_{BET}) (m^2/g), and the total pore volume (p/p_o) (cm^3/g) of biochar-NH_2 were estimated from the BET using BELSORP–Mini II, BEL Japan, Inc. [46, 47]. The micropore surface area (S_{mi}) and volume (V_{mi}) as well as the mesopore surface area (S_{mes}) and volume (V_{mes}) of biochar-NH_2 were also determined using "Barrett–Joyner–Halenda (BJH) procedures." While the BJH method was used to compute the pore size distribution from the desorption isotherm [48], a scanning electron microscope (SEM) (QUANTA 250) attached with a dispersive X-ray spectrometer (EDX) was employed to analyze the morphology and elementary composition of the synthesized biosorbent. The "Fourier transform infrared (FTIR) spectroscopy VERTEX70" connected to a Platinum ATR unit model V-100 was used to detect the IR-observable functional groups on the biochar-NH_2 surface in the wavenumber range of 400–4000 cm^{-1}. The thermal analysis was executed using the SDT650-Simultaneous Thermal Analyzer instrument (50–1000 °C) with a 5 °C per minute ramping temperature.

2.4 Batch adsorption experiment

The sorption capacity, thermodynamic, and kinetic characteristics of biochar-NH_2 were determined from batch experiments. For a certain time, various flasks comprising of varying initial concentrations of Cu(II) solution (100 mL) and fixed weights of biochar-NH_2 were shaken at 200 rpm. The pH of the various solutions was modified to the necessary values using 0.10 M HCl or NaOH. The solution pH was kept constant throughout the sorption equilibrium studies. After separating approximately 0.1 mL of the solution from the adsorbent, the concentration of Cu(II) was determined at various time intervals. The final concentration of Cu(II) ion in the filtrate was estimated using diethyldithiocarbamate as a complexing reagent in a spectrophotometer set at $\lambda_{max} = 460$ nm [20, 44, 45]. Equation (1) was used to determine the amount of Cu(II) adsorbed by a unit mass of adsorbent at various times (t).

$$q_t = \frac{(C_o - C_t)}{W} V \quad (1)$$

q_t, C_o, C_t, V, and W represent the sorption capacity of the adsorbent at time t (mg/g), the initial concentration of Cu(II) (mg/L), the residual concentration of the Cu(II) over a time (t) (mg/L), the volume of Cu(II) ion solution (L), and the mass of the sorbent (g).

The impact of pH on the Cu(II) sequestration by biochar-NH_2 was considered by the addition of 0.10 g of the sorbent to 100 mL of 200 mg/L of Cu(II) solutions at different initial pH values ranging between 2.20 and 5.60, and 0.10 M HCl or NaOH solutions were used to adjust the solution pH values. The mixtures were shaken at 200 rpm speed and sampled at various interval times. The equilibrium concentration of Cu(II) ion was then evaluated.

The effect of biochar-NH_2 dose on Cu(II) ion sequestration and the isotherm studies were investigated using various beginning concentrations of Cu(II) solutions (ranging between 50 and 300 mg·L^{-1}). Cu(II) ion concentrations were determined at intervals in mixes of 1 to 3 g/L biochar-NH_2 and Cu(II) ion solutions of varied starting concentrations were stirred at 200 rpm at room temperature. All adsorption studies were done in triplicate, and the data are given as a mean.

The UV spectrophotometer was used to analyze the copper (II) ion concentration in the wastewater due to the simplicity of this technique in measuring the concentration of copper. As well as the effectiveness and sensitivity of this method, also this method is considered a cost-effective solution to the field test study. However, the literature for this analysis has been reported in our previous studies, see references [20, 44, 45] as well as the references in them. The unmodified WMP was tested against the unmodified biochar for Cu(II) ion removal and it gave very low or negative removal of Cu(II) ion from water.

3 Results and discussion

3.1 Biochar-NH_2 characterization

The FTIR was employed to analyze the functional groups present in the created biochar-NH_2 (Fig. 1), and the raw WMP was compared to the WMP biochar (biochar-NH_2). The FTIR spectra reveal alterations in their functional groups. The band at 3267 cm^{-1} indicates the O–H stretching vibration present in the watermelon peel, whereas the band at 3186 cm^{-1} signifies both the OH and NH_2 groups in the biochar-NH_2 sample (Fig. 1). The large adsorption peak noticed at 2922 cm^{-1} specifies the presence of $–CH_2$ stretching groups in WMP, which were not observed in biochar-NH_2 (Fig. 1). The adsorption peak at 1726 cm^{-1} can be ascribed to the C = O stretching of ester groups in WMP, which was transformed to a band at 1554 cm^{-1} by the addition of an amino group in biochar-NH_2 (Fig. 1). However, as compared to raw WMP, the band at 1554 cm^{-1} in biochar-NH_2 was extremely strong, showing the existence of a significant quantity of NH_2 functional group in the newly created biochar-NH_2. The presence of bands at 1598 cm^{-1} indicates the C = O stretching vibration of β-ketone, which was nearly completely absent in watermelon skin. This reflects the stretching vibration of –C = C– (Fig. 1). The peak at 1405 cm^{-1} corresponds to the C-O functional group in watermelon skin, while the band at 1371 cm^{-1} in biochar-NH_2 indicates the stretching vibration of the amino group (NH_2) (Fig. 1). The oxygenated carbon chain peaks

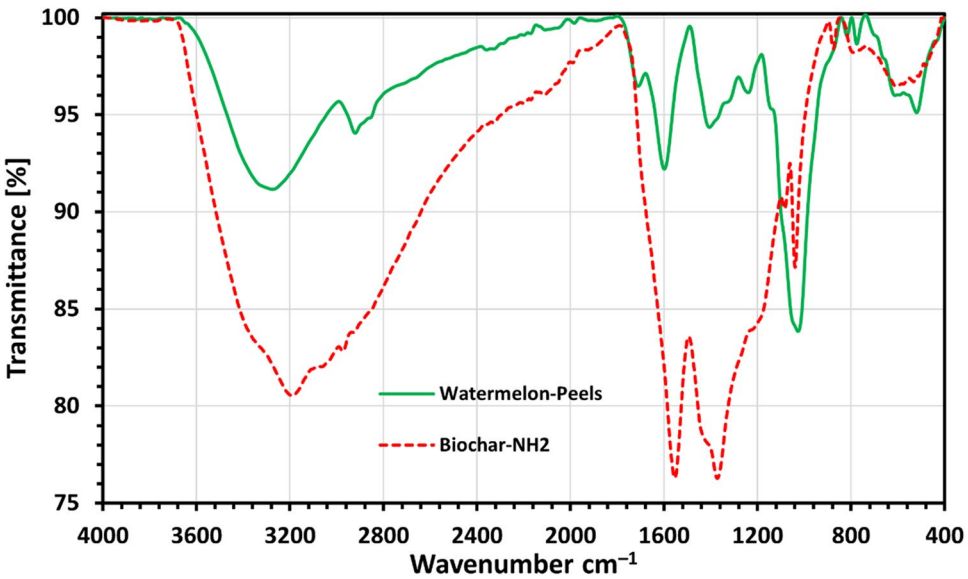

Fig. 1 FTIR analysis of raw WMP and biochar-NH_2

at 1024 cm^{-1} were observed in WMP but were reduced in biochar-NH_2 at 1039 cm^{-1} [49, 50].

The influence of the amine groups on the surface properties of biochar-NH_2 produced from WMP was examined using nitrogen adsorption–desorption isotherms. The BET and BJH procedures were utilized for computing the specific surface area and mesopore area. The textural parameters of biochar-NH_2 are shown in Fig. 2, which include the "BET specific surface area, total pore volume, mean pore diameter, monolayer volume, mesopore area, mesopore volume, and mesopore distribution peak." In general, the BET-specific surface area of biochar-NH_2 was 12.26 m^2/g. The monolayer volume value of biochar-NH_2 was 2.82 cm^3 (STP) g^{-1}. The total pore volume value of biochar-NH_2 was 0.012 cm^3/g. The mean pore diameter of biochar-NH_2 was 5.94 nm (mesopores). The meso surface area of biochar-NH_2 was 12.96 $m^2\ g^{-1}$, the mesopore volume value of biochar-NH_2 was 0.021 $cm^3 \cdot g^{-1}$, and the mesopore distribution peak value of biochar-NH_2 was 1.66 nm (Fig. 2) [49, 50].

Figure 3 shows the SEM of raw WMP and biochar-NH_2. The biochar-NH_2 seems clean and free of any particle contaminants, as shown in Fig. 3b, and no impairment to the pores of the raw WMP was seen after treatment with heated NH_4OH.

The chemical compositions of the biochar-NH_2 samples were evaluated using an EDX, and the elements % are reported in Table 1. The main elements in the biochar-NH_2 were oxygen (O), nitrogen (N), carbon (C), sulphur (S), and calcium (Ca). O, N, and C account for 13.36%, 24.88%, and 59.28% of the biosorbent.

The "thermal gravimetric analysis (TGA)" was utilized to determine the effect of the structural changes between the WMP and biochar-NH_2 on their degradation behavior. Each sample was prepared in an N_2 environment, employing a temperature ranging from ambient temperature to 1000 °C. TGA and DTA analytical curves for raw WMP and biochar-NH_2 are shown in Fig. 4a. Initial weight loss peaks for both materials were noticed before at 100 °C, and this was attributable to H_2O volatilization. The second weight loss peak (> 100 °C) for raw WMP was ascribed to the breakdown of several acidic oxygen functional groups. However, acidic groups, for example, anhydrides, carboxylic, and lactones, degrade at lesser temperatures, and acidic groups, for example, phenol, decompose at higher temperatures. The second weight loss in the case of biochar-$NH_2$was noticed at above 180 °C. At temperatures up to 450 °C, the amine-modified sample was observed to uninterruptedly lose weight gradually, whereas raw WMP reaches a modest weight

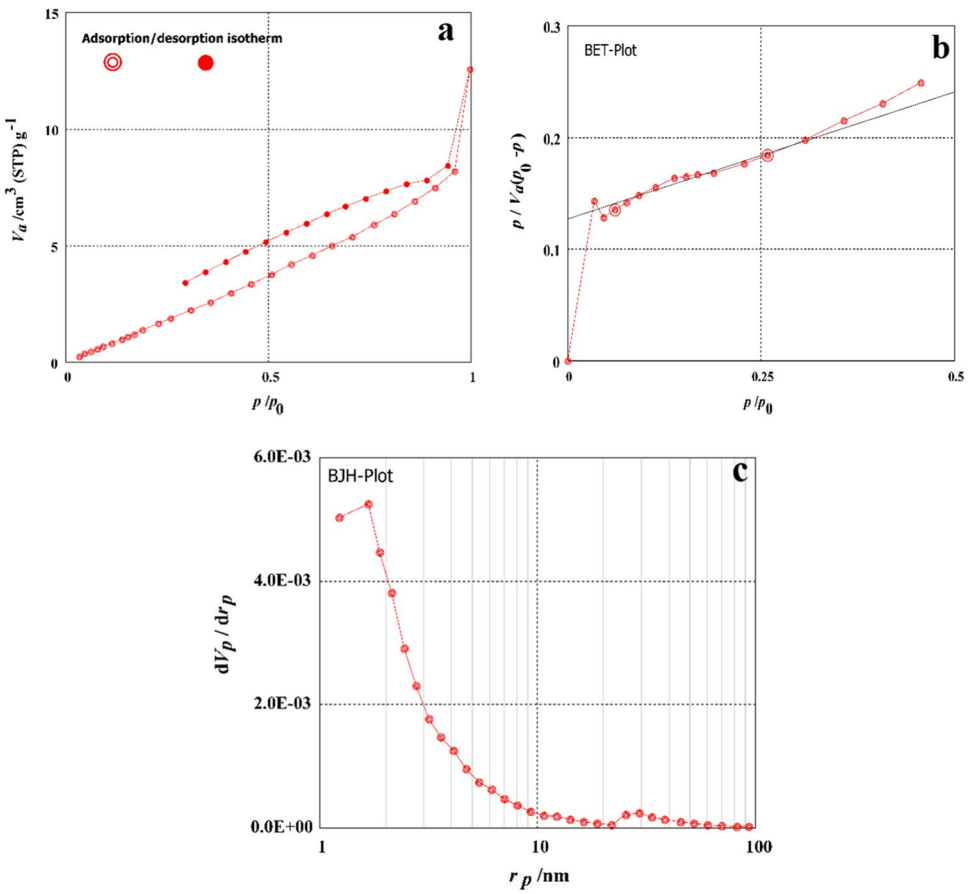

Fig. 2 **a** Sorption/desorption, **b** BET analysis, and **c** BJH analysis plot of biochar-NH_2

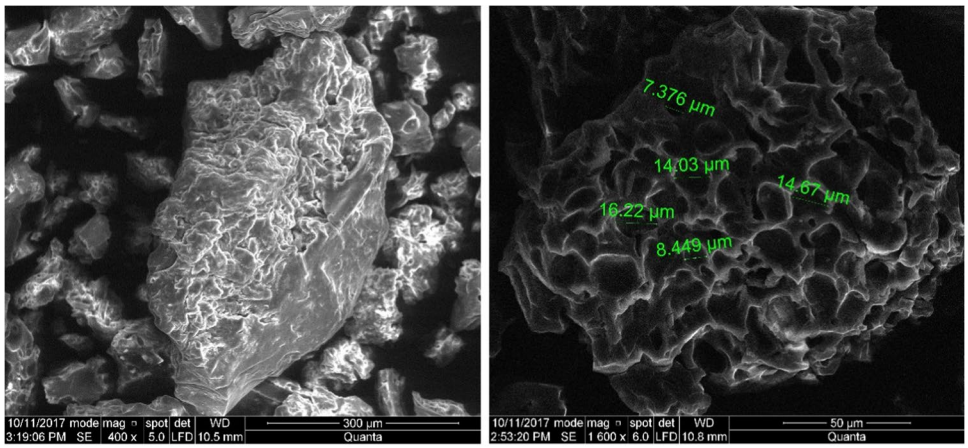

(a) **(b)**

Fig. 3 SEM image of **a** WMP and **b** biochar-NH_2

Table 1 EDX analysis data of biochar-NH_2

Biochar	Biochar-NH_2	
Elements	Wt (%)	At (%)
C	59.28	65.68
N	13.36	12.70
O	24.88	20.70
S	1.20	0.50
Ca	1.28	0.42

loss plateau. Both TGA curves converged at temperatures greater than 450 °C due to carbon breakdown within the biochar framework. At a final temperature of 1000 °C, various weight losses of biochar-NH_2 and WMP were observed, with weight loss percentages of 27.95% and 39.56%, respectively. The weight stayed within the range for WMP and biochar-NH_2, and with 12.62% and 52.80% obtained, which is indicative of a more stable biochar-NH_2 than raw WMP [49, 50].

The DTA of WMP and biochar-NH_2 is shown in Fig. 4a. As shown in Fig. 4a, the DTA curve of the WWP (red) sample exhibits six distinct peaks at flow temperatures (Tf 769, 178, 251, 292, 426, and 872 °C), whereas the DTA curve of the biochar-NH_2 sample revealed only two distinct degradation peaks at flow temperatures (Tf 767 and 477 °C) and the thermal transitions can be used to compare materials using differential scanning calorimetry (DSC).

The DSC profiles of raw WMP and biochar-NH_2 are shown in Fig. 4b. Both samples exhibited crystallization temperatures T_C below 100 °C, which are attributable to water molecule crystallization. Other phase transitions are not observed in biochar-NH_2. The raw WMP and biochar-NH_2 reach the melting point as the temperature rises. However, fresh WMP melts between 297.62 and 422.87 °C, whereas biochar-NH_2 melts at 486.76 °C. WMP in its raw state has a lower transition temperature than Melon-B biochar. The higher transitional temperatures induced a larger degree of crystallinity, which provided structural stability and increased the gelatin resistance of the grains.

3.2 pH effect

The value of the solution pH indicates the level of H^+ concentration in water and the concentration of H^+ significantly impacts the electrostatic interaction and ion exchange [51, 52]. The extent of the sorbent protonation is also evaluated based on the pH, which subsequently affects the different functional groups' charges and the sorption capacity of the sorbent. Another important factor that indicates the efficiency of the sorbent and which depends on the pH of the treated water is the point of zero charge (pH_{pzc}). It is an important sorption process parameter due to it allowing the identification of the pH value at which the charges at the sorbent surface will alter from anionic ($> pH_{pzc}$) to cationic ($< pH_{pzc}$). The importance of this parameter depends on the analyte chemical composition and it is possible to determine what pH range should experiments be conducted as well as the effect that this cause in huge-scale applications using this parameter [53–55]. Anionic and cationic species sorption was promising when the sorbent surface was either positively or negatively charged due to the solution pH being less or greater than the pH_{pzc}. The sorption of cations was favorable when the $pH > pH_{PZC}$, while anions sorption was favorable when the $pH < pH_{PZC}$ [56, 57]. The pH_{pzc} of the synthesized biosorbent in this study was determined to be 5.2 (Fig. 5a).

The main species of Cu in the pH range of 3–4 are Cu^{2+} and $CuOH^+$ and above the pH value of 5, Cu appears as $Cu(OH)_2$ [30]. It was found that the % of Cu(II) confiscated to the biochar-NH_2 was rapid at the beginning with more than 95% of Cu(II) ion sorption taking place within the first 120 min. The consequence of pH on the sorption of Cu(II) ion onto

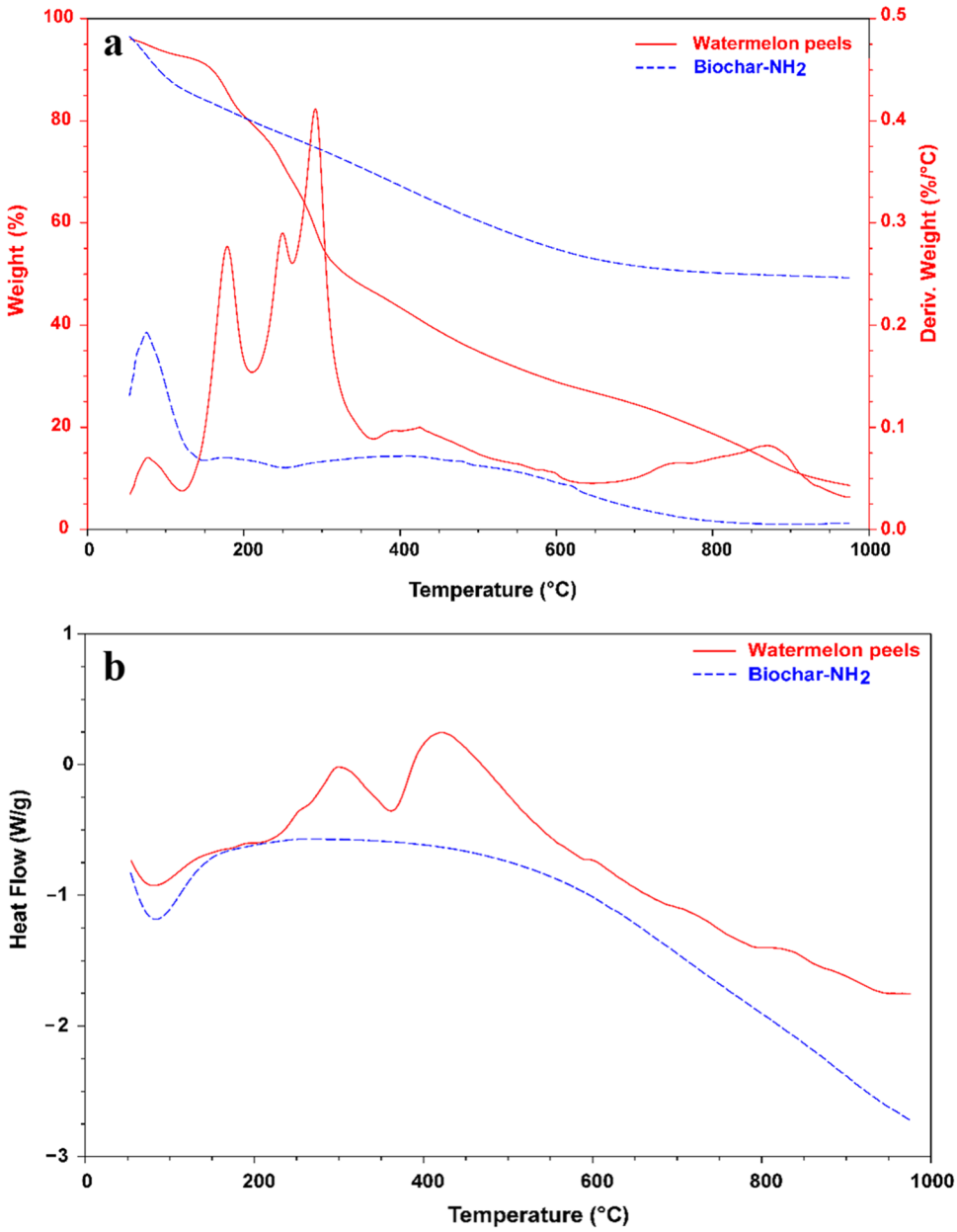

Fig. 4 **a** TGA and DTA, and **b** DSC analyses of raw WMP and biochar-NH_2 samples

the biochar-NH_2 was explored over the pH values of 2–5 and the % of Cu(II) removed to the biochar-NH_2 was observed to improve with an intensification in the pH of the solution over a time range. The ideal confiscation percentage of Cu(II) ion to the biochar-NH_2 was noticed at a pH value of 5.6 (Fig. 5b). At low pH values, the sorbent surface was protonated with excessive H^+ (positively charged) causing sturdy electrostatic repulsion between positively charged Cu(II) specie and the protonated charged active sites in the biochar-NH_2. With an increase in the solution pH to higher pH values, the active sites on the surface of the sorbent become deprotonated and become negatively charged. Hence, the negatively charged sites on the biochar-NH_2 surface were electrostatically attracted to the positively charged Cu(II) specie, leading to enhanced confiscation of Cu(II) ion. Under acidic circumstances (low pH), the sorption of cationic metals such as Cu(II) was reduced owing to the intense contest from the H^+ ions and protonated functional groups for the positively charged sites of the sorbent. With the increase in the solution pH, the number of H^+ reduced and hence the sorption of Cu(II) ion [56]. Similar findings were reported by Gupta and Gogate [16] and Phuengphai et al. [14].

3.3 Effect of sorbent dosage and initial Cu(II) concentration

A key factor that controls the sorbent confiscation capacity at the operational conditions is the optimization of the sorbent dosage [58–60]. The effect of the sorbent dosage on the

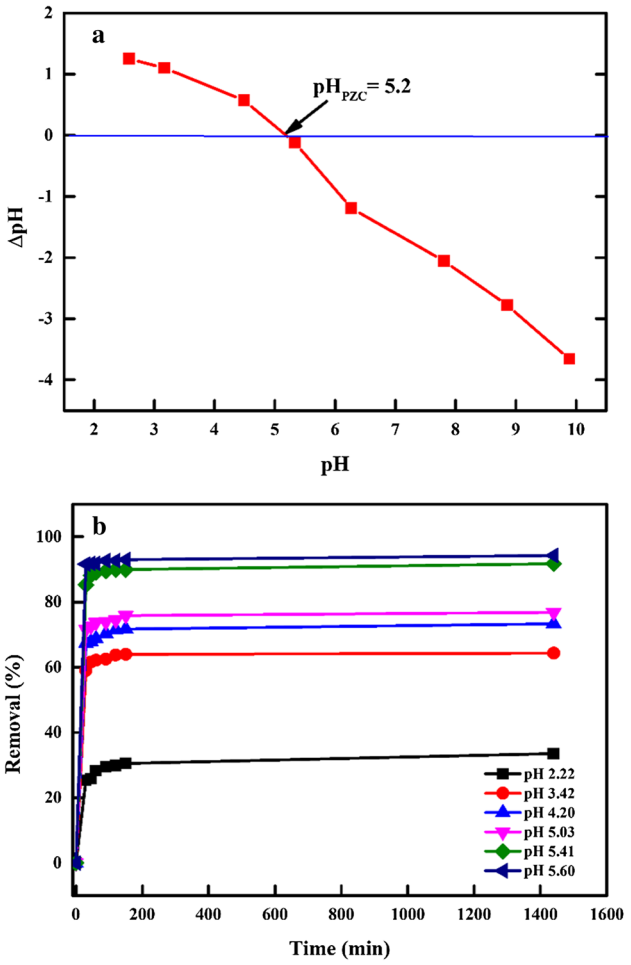

Fig. 5 **a** The pH_{pzc} of the biochar-NH_2 and **b** impact of pH on the sorption of Cu(II) ion

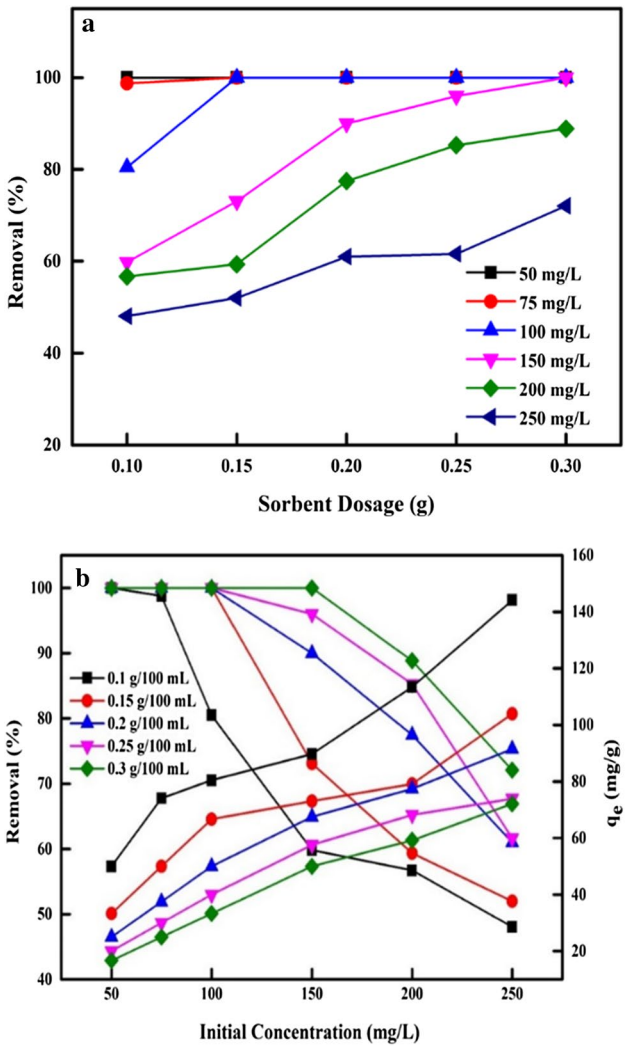

Fig. 6 **a** Impact of sorbent dosage (0.1–0.3 g/100 mL) on the removal/subtraction of Cu(II) ion of initial concentration ranged between 50 and 250 mg·L^{-1}; **b** impact of initial concentration (50–250 mg·L^{-1}) on the confiscation of Cu(II) to the biochar-NH_2

sorption of Cu(II) to the biochar-NH_2 is shown in Fig. 6a. It was noticed that an increase in the amount of sorbent used from 1 to 3 g L^{-1} led to an intensification in the percentage of Cu(II) eliminated at various initial Cu(II) concentrations. With a rise in the initial concentrations of Cu(II) ion, the percentage of Cu(II) removed decreased from 100 to 45% using 1 g L^{-1} of biochar-NH_2 dosage as the initial concentration was improved from 50 to 250 mg L^{-1} and 99–68% using a biochar-NH_2 dosage of 3 g L^{-1} as the initial concentration was improved from 50 to 250 mg L^{-1}. Such performance is obvious in the increased sorbent capacity for metal uptake when the sorbent dosage is increased and which corresponds to the enhanced number of active sites accessible for the uptake of metal ions [14, 61]. This decrease in the confiscation % with an upsurge in the initial concentration of the metal ions was ascribed to the available active sites being insufficient for the complete sorption of all metal ions and the formation of aggregates which reduces the effective surface area for sorption at elevated sorbent dosage [62, 63].

A key role is played by the initial metal concentration in water-soluble solutions as it promotes the driving force in overcoming the metal ions mass transfer resistance between the solid sorbents and water-soluble solution [64, 65]. Figure 6b shows the impact of initial Cu(II) concentrations on the % of metal ions confiscated at varying initial concentrations ranges of 50–250 mg L^{-1}. It was noticed that the rate of Cu(II) sorption was a function of the initial concentration of the metal ions. With the increase in the initial concentration of the metal ions from 50.00 to 250 mg L^{-1}, the % of Cu(II) ion removed decreased from 100.00 to 72.00% using a sorbent dosage of 3 g L^{-1} and 1 g L^{-1}, and the % of Cu(II) removed also decreased from 100 to 46%. Superior sorption noticed at low concentration was ascribed to the elevated driving

force in terms of accessible binding sites. While at an elevated concentration of metal ions, there were contests for the binding sites by the excess Cu(II) ion and resulting in most Cu(II) ion left unabsorbed from the solution owing to the rapid permeation of the active binding sites on the sorbent surface. Also, such actions can be ascribed to the enhanced amount of the sorbate to the rigid number of accessible active sites on the sorbent surface, hence a low sorption percentage was obtained due to the obstruction of the interaction between the unabsorbed metal ions and the biosorbent sites [66]. Also, the equilibrium sorption capacity was noticed to improve with rising initial Cu(II) concentration (50–250 mg L^{-1}) at the various dosage of sorbent used (0.1–0.3 g/100 mL). This rise was attributed to the high impact between the sorbate particles and the active sorbent sites, therefore enhancing the driving force of the sorbate to the sorbate surface [9, 67].

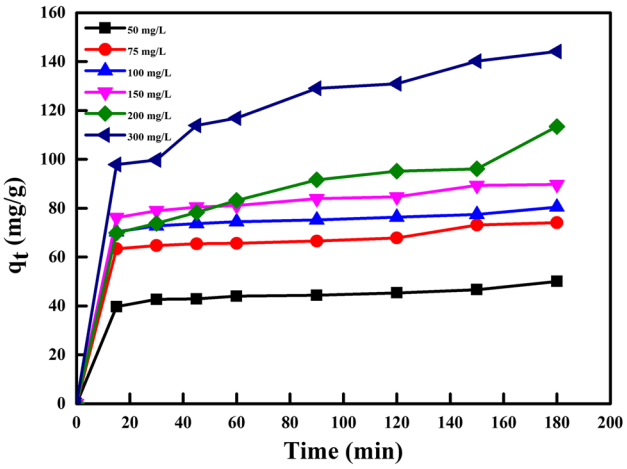

Fig. 7 Contact time effect on the sorption of Cu(II) (50–300 mg L^{-1}) by biochar-NH_2 (1 g L^{-1})

3.4 Effect of time and kinetic models

A key and efficient factor in the sorption process is the time duration between the surface of the sorbent and the pollutants, which plays an efficient role in the kinetics and sorption process speed [68]. The study of kinetics is built on the frequency of sorbate contained in solution confiscated by the sorbent relative to the time of contact between them. This frequency of sequestration of the analytes can be impacted by different factors like pH, size of the particle, concentration of sorbate, and temperature. In the bio-treatment of various WW, sorption kinetics remains an important factor when a sorbent to be used is being selected [53]. The rate of Cu(II) sorption to the biochar-NH_2 was enhanced rapidly within the first 15 min (indicative of a sturdy affinity between the sorbate and sorbent, which was swift) and sorption equilibrium was attained in 60 min as shown in Fig. 7. The initial swift uptake was ascribed to the huge amount of uninhabited sites presence and with the advance of time, sorption equilibrium was attained and further, than this, no more Cu(II) ions were sorbed [69].

To evaluate the sorption process applicable to the treatment of Cu(II) effluent, kinetic investigations were conducted. The kinetics of Cu(II) sorption was assessed employing some kinetic models (KNMs) such as the pseudo-first-order (PFO), PSO, Elovich, and intraparticle diffusion models (Fig. 8) [70–73]. The PFO model is useful in defining a scientific correlation between the rate of sorption and mass sorbed based on the assumption of membrane diffusion, while the PSO model proposes that the process of sorption is controlled by chemisorption, which entails the valence sharing or the electrons exchange between the sorbed species and the sorbent [74]. The linearized forms of both PFO and PSO models are depicted by Eqs. (2) and (3):

$$\log\left(q_e - q_t\right) = \log\left(q_e\right) - \frac{k_1 t}{2.303} \tag{2}$$

$$\frac{t}{q_t} = \frac{1}{k_2 q_e^2} + \frac{1}{q_e}(t) \tag{3}$$

q_e, q_t, k_1, and k_2 represent the adsorption amount at equilibrium and time t, respectively (mg g^{-1}), the sorption PFO-rate constant (min^{-1}), and PSO sorption rate constant ($g{\cdot}mg^{-1}{\cdot}min^{-1}$). The plot of log ($q_e - q_t$) against t gives a linear relationship graph and constant k_1 and q_e are determined from the slope and intercept, respectively. While from the linearity plot of (t/q_t) against t, the k_2 and q_e are defined from the slope and intercept, respectively [75].

The Elovich model is generally used when it is presumed that the solid surface is energetically diverse and the linearized form of this model is depicted by Eq. (4) [76].

$$q_t = \frac{1}{\beta}\ln(\alpha\beta) + \frac{1}{\beta}\ln(t) \tag{4}$$

where α, β represent the initial sorption rate (mg g^{-1} min^{-1}) and the degree of the surface coverage and the activation energy chemisorption (g mg^{-1}). These coefficients are determined from the plot of q_t against ln t [77].

The intraparticle diffusion model was applied to analyze the behavior of initial sorption. This model is generally utilized in three forms, which include getting a plot with a linear line that is compelled to pass through the basis, a multi-linear plot with two or three stages, comprising of the entire process of external surface sorption and steady sorption where intraparticle diffusion is controlled, and the third stage which involves the solutes slow movement from huge pore to micropores, hence causing the slow rate of sorption

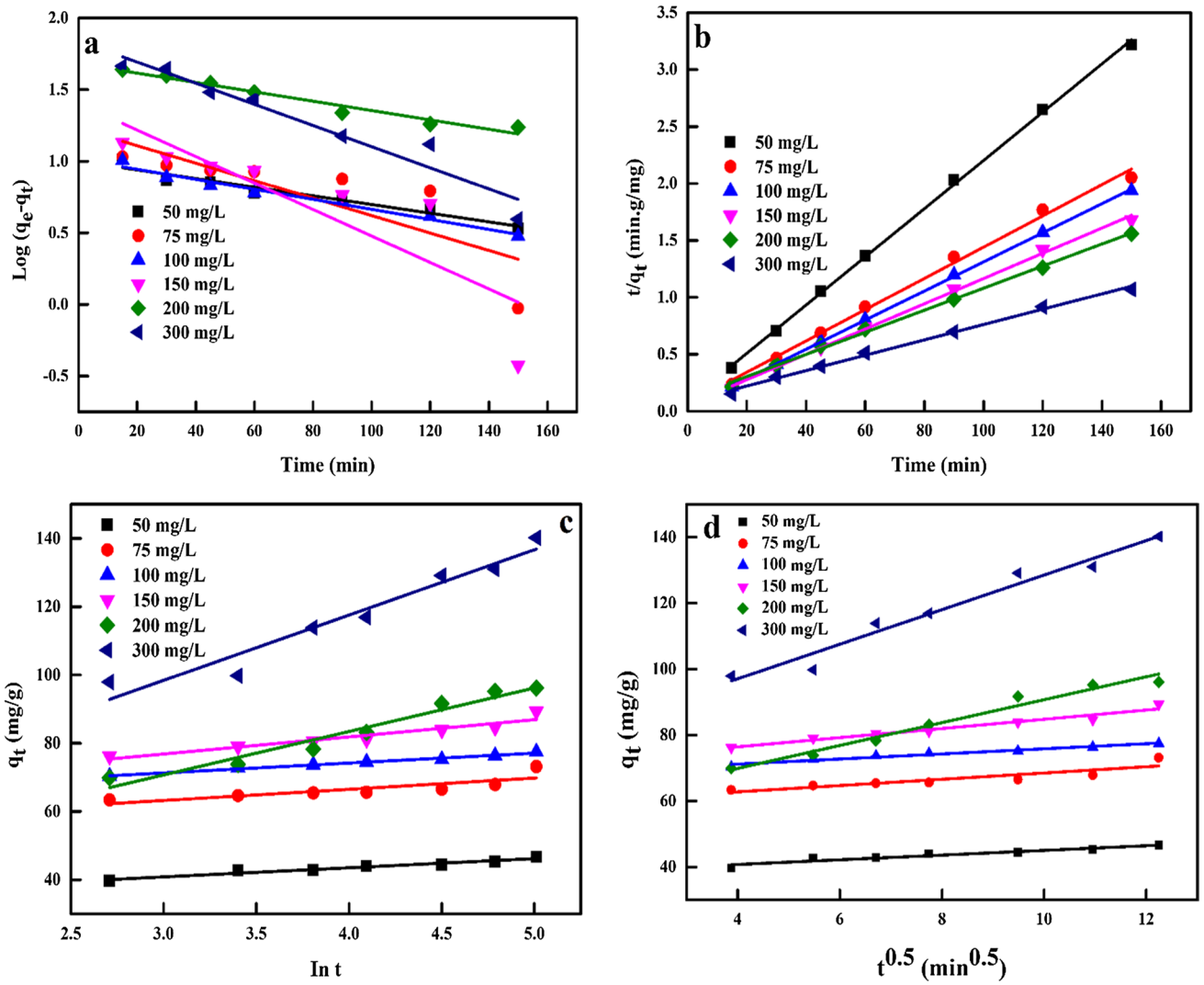

Fig. 8 Kinetic (KNM) of Cu(II) sorption to biochar-NH_2 **a** PFO model, **b** PSO model, **c** Elovich model, and **d** intraparticle diffusion model

and final form involves a linear line being obtained but does not certainly pass via the origin, hence there is an intercept. The intercept is comparative to the thickness of the boundary layer and the bigger the intercept, the larger the impact of the boundary layer [78]. The linearized form of the intraparticle diffusion model is given by Eq. (5).

$$q_t = k_{dif} t^{0.5} + C \quad (5)$$

k_{dif} and C represent the intraparticle diffusion rate constant (g mg^{-1} min^{-1}) and the intercept of the plot of q_t against $t^{0.5}$ and the boundary layer effect or surface sorption [79]. The PFO, PSO, Elovich, and intraparticle diffusion models were utilized in this study to get an improved understanding of the sorption outline achieved by the biochar-NH_2 from the acquired data and the calculated kinetic parameters are summarized in Tables 2 and 3. The best fit model that described the sorption process of Cu(II) was selected based on the linear regression correlation coefficient (R^2) value. In terms of R^2, the PSO model best describes the sorption process of Cu(II) and which was in agreement with the experiment data ($R^2 > 0.99$). A good linear correlation was given between the PSO model and the experimental data as shown in Fig. 8b. Also, the equilibrium sorption capacities (q_e) determined from the contact time study were consistent or close with that of the theoretical q_e values determined from the PSO model. Hence, it is assumed that the sorption process comprises of a chemisorption process in rate-limiting stages [80]. Cu(II) confiscation can also include both chemisorption and physisorption processes, where the chemisorption is typified by the chemical reactions based on the electrons exchange among the sorbent and the species of interest, while the physisorption was due to Van der Waals forces, which are weaker interactions [53].

Table 2 Parameters of PFO and PSO models fitted for the sorption of Cu(II) to the biochar-NH_2

Parameter			PFO KNM			PSO KNM			
Biochar-NH_2 conc. (g L^{-})	Cu(II) (mg L^{-1})	q_e (exp.)	q_e (calc.)	k_1 ($\times 10^3$)	R^2	q_e (calc.)	k_2 ($\times 10^3$)	H	R^2
1.0	50.00	50.00	10.02	6.91	0.936	47.17	5.35	11905	0.999
	75.00	74.06	17.02	14.05	0.673	72.99	2.76	14728	0.995
	100.00	80.47	10.34	8.06	0.973	78.13	5.10	31153	1.000
	150.00	89.72	25.29	21.19	0.740	90.09	2.25	18248	0.998
	200.00	113.42	47.90	7.60	0.964	103.09	0.85	9025	0.997
	300.00	144.13	69.23	17.04	0.938	149.25	0.52	11494	0.995
1.5	50.00	33.33	6.53	11.75	0.965	33.67	5.27	5970	0.997
	75.00	50.00	6.70	8.29	0.933	48.54	7.83	18450	1.000
	100.00	66.67	8.09	10.36	0.717	66.23	4.64	20367	0.998
	150.00	73.08	10.44	9.44	0.914	70.92	4.02	20243	0.999
	200.00	79.12	33.43	17.73	0.737	79.37	1.33	8403	0.989
	300.00	103.97	65.13	23.72	0.898	111.11	0.63	7776	0.993
2.0	50.00	25.00	4.89	9.44	0.936	25.06	6.67	4191	0.995
	75.00	37.50	5.36	11.05	0.947	37.04	8.83	12107	1.000
	100.00	50.00	4.40	9.21	0.951	50.00	7.92	19802	0.999
	150.00	67.49	6.19	9.90	0.847	67.57	5.95	27174	0.999
	200.00	77.46	23.96	29.94	0.955	79.37	2.78	17513	1.000
	300.00	91.50	27.03	9.67	0.976	88.50	1.51	11806	0.998
2.5	50.00	20.00	3.18	8.52	0.912	20.16	9.65	3923	0.998
	75.00	30.00	2.65	8.29	0.941	29.50	18.87	16420	1.000
	100.00	40.00	3.18	8.52	0.938	40.16	10.10	16287	0.999
	150.00	57.60	6.29	14.51	0.653	57.14	8.30	27100	0.999
	200.00	68.21	10.35	14.05	0.856	68.03	4.72	21834	0.999
	300.00	73.95	22.93	15.66	0.971	75.19	1.68	9524	1.000
3.0	50.00	16.67	2.21	8.31	0.756	16.81	13.16	3717	0.998
	75.00	25.00	1.84	8.52	0.984	24.63	28.77	17452	1.000
	100.00	33.33	1.98	5.99	0.826	33.33	15.18	16863	1.000
	150.00	50.00	2.72	6.68	0.940	50.00	12.12	30303	1.000
	200.00	59.22	5.847	14.05	0.896	59.17	8.45	29586	1.000
	300.00	72.08	10.34	15.20	0.927	71.94	4.60	23810	1.000

3.5 Isotherm model

For a better insight into the sorption trend occurring with various materials empirically and obtaining key factors that reveal the sorption mechanism, theoretic isotherm models (ISMs) are used on the data. In this study, various ISMs like LGR, Freundlich (FRH), and Temkin (TMN) models were utilized to determine the sorption trend [53, 70, 81]. The LGR model presumes that monolayer sorption happens on a uniform surface with a limited number of sites for sorption and trivial common interactions between the molecules adsorbed. The linearized form of this ISM (type 1) is given by Eq. (6).

$$\frac{C_e}{q_e} = \frac{1}{bq_m} + \frac{C_e}{q_m} \tag{6}$$

C_e, q_e, q_m, and b represent the equilibrium concentration of metal ions (mg L^{-1}), the number of metal ions sorbed at equilibrium (mg g^{-1}), the optimum amount of metal ions removed which corresponds to the overall coverage of the sorption sites (mg g^{-1}), and LGR constant that relates to energy sorption (L mg^{-1}). The values of b and q_m are defined from the plot of C_e/q_e against C_e intercept and slope as shown in Fig. 9 [81]. The FRH model is relevant to sorption processes that happen on the diverse surface and this model gives an expression that describes

Table 3 Parameters of Elovich and intraparticle diffusion models fitted for the sorption of Cu(II) to the biochar-NH_2

Sorbent dose (g L^{-1})	Cu(II) conc. (mg L^{-1})	Elovich			Intraparticle diffusion		
		β	α	R^2	K_{dif}	C	R^2
1.0	50	0.374	5.688×10^{5}	0.9562	0.710	37.914	0.9207
	75	0.303	3.513×10^{7}	0.7068	0.950	58.992	0.8033
	100	0.346	7.37×10^{9}	0.9869	0.773	68.090	0.9640
	150	0.198	1.05×10^{6}	0.911	1.395	70.841	0.9553
	200	0.079	1.64×10^{2}	0.9582	3.472	56.003	0.9745
	300	0.052	1.64×10^{2}	0.9420	5.237	76.130	0.9664
1.5	50	0.454	3.65×10^{4}	0.9245	0.604	25.421	0.9513
	75	0.506	4.56×10^{8}	0.9551	0.522	41.849	0.9125
	100	0.544	1.98×10^{13}	0.5905	0.545	58.172	0.7109
	150	0.293	1.73×10^{7}	0.9246	0.924	58.940	0.9294
	200	0.125	6.25×10^{2}	0.8864	2.177	49.657	0.8981
	300	0.067	8.90×10^{1}	0.9519	4.073	53.787	0.9796
2.0	50	0.641	4.93×10^{4}	0.8438	0.436	18.948	0.9014
	75	0.603	3.79×10^{7}	0.9498	0.440	31.251	0.9158
	100	0.691	5.24×10^{12}	0.8410	0.406	44.413	0.9079
	150	0.576	3.74×10^{14}	0.7626	0.493	60.345	0.8409
	200	0.172	2.59×10^{4}	0.9552	1.509	60.158	0.8815
	300	0.140	6.10×10^{3}	0.9253	1.980	60.910	0.9791
2.5	50	0.784	3.75×104	0.9274	0.347	15.486	0.9364
	75	1.554	1.77×10^{17}	0.9078	0.179	27.003	0.9558
	100	0.860	4.08×10^{12}	0.8629	0.326	35.653	0.9276
	150	0.820	7.59×10^{17}	0.7131	0.347	52.122	0.7901
	200	0.279	3.27×10^{6}	0.8724	0.919	56.217	0.7864
	300	0.158	3.15×10^{3}	0.8937	1.767	50.602	0.9540
3.0	50	1.023	1.18×10^{5}	0.9457	0.264	13.267	0.9425
	75	1.942	1.39×10^{18}	0.9831	0.139	22.817	0.9754
	100	1.296	1.64×10^{16}	0.8745	0.216	30.396	0.9329
	150	1.044	1.42×10^{20}	0.8174	0.267	46.227	0.8681
	200	0.627	7.90×10^{13}	0.9457	0.436	53.182	0.9702
	300	0.309	7.32×10^{7}	0.9352	0.868	60.809	0.9229

the heterogeneity of a surface and active sites and their energies exponential distribution. The linearized form of this model is given in Eq. (7) [70].

$$\log q_e = \log K_F + \frac{1}{n}\log C_e \tag{7}$$

K_F and n represent the FRH constant and heterogeneity factor, which relates to the sorption intensity. The plot log q_e against log C_e yields the intercept (log K_F) and slope ($1/n$). For the positive sorption process, n value should be $1 < n < 10$ [19, 82], while the TMN model takes into description the impacts of implicit sorbate/sorbate interactions on the sorption procedure. It is presumed that all molecules sorption heat in the layer diminishes linearly due to the enhanced surface coverage. This model is simply applicable for an intermediary range of concentrations of ions. The linearized form of this model is given by Eq. (8) [83].

$$q_e = B_T \ln A_T + B_T \ln C_e \tag{8}$$

where

$$B_T = \frac{RT}{b} \tag{9}$$

A_T, b, R, and T represent the TMN isotherm equilibrium binding constant (L g^{-1}), the TMN constant relating to the heat of sorption (J mol^{-1}), the universal gas constant (8.314 J mol^{-1} K^{-1}), and temperature at 298 K. The plot of q_e against ln C_e allows for the estimation of the TMN constants [69]. Table 4 shows the determined parameters of ISMs with their respective R^2 describing the sorption of Cu(II) to biochar-NH_2. As observed in Table 4, the determined values of the R^2 show that the most suitable model that described the sorption of Cu(II) was the LGR model with an R^2 value of 0.944 when compared to FRH and TMN models. Hence, Cu(II) ion sequestration to the biochar-NH_2

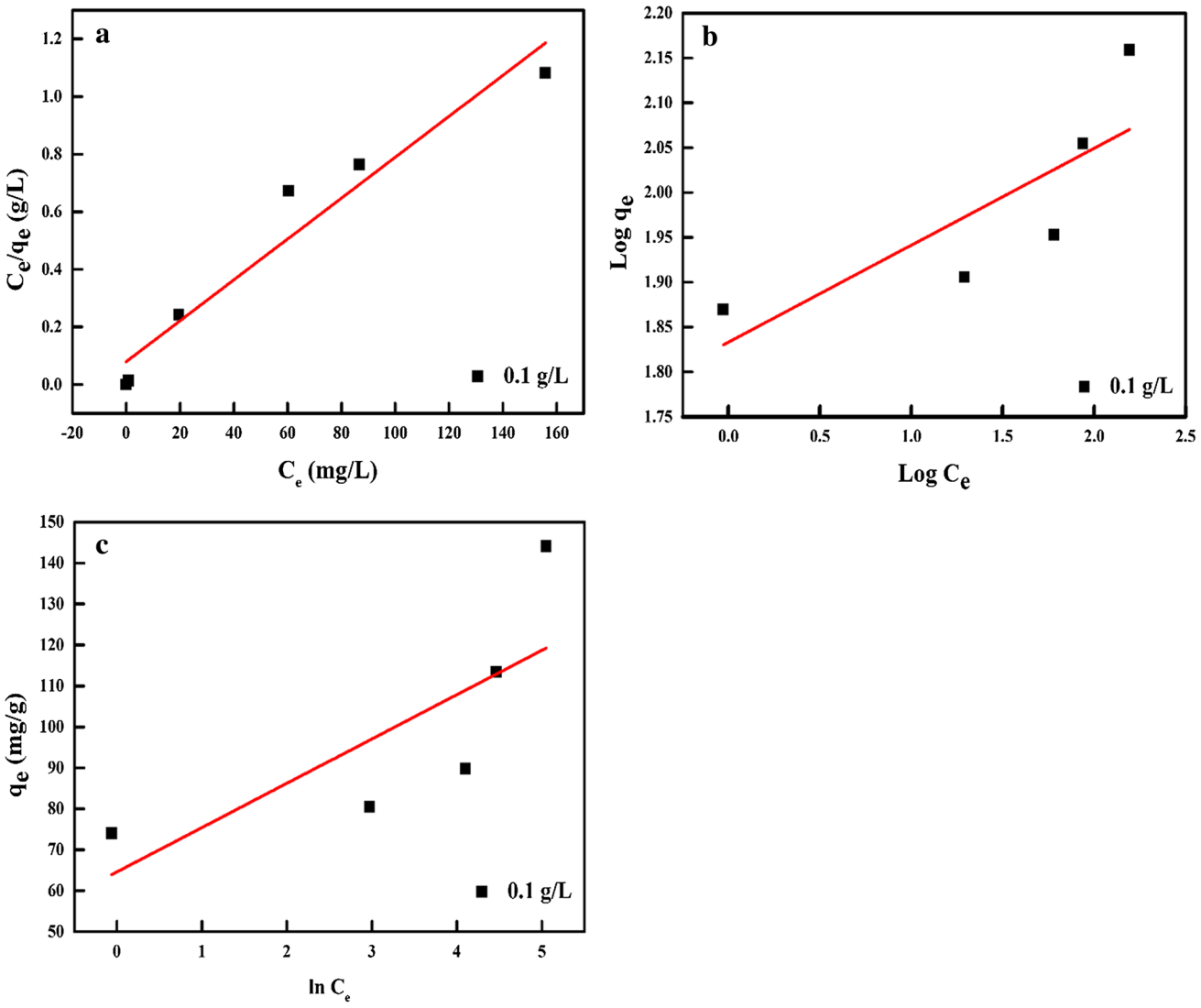

Fig. 9 Plots of **a** LGR ISM, **b** FRH ISM, and **c** TMN ISM for the sorption of Cu(II) to biochar-NH_2

Table 4 LGR, FRH, and TMN sorption isotherm parameters for Cu(II) confiscation onto biochar-NH_2

ISM	Isotherm parameter	Biochar-NH_2 concentrations 1.0 g L^{-1}
LGR	q_m	140.85
	b	0.09
	R^2	0.944
FRH	$1/n$	0.141
	K_F (mg/g)/(L/mg)$^{1/n}$	59.020
	R^2	0.769
TMN	A_T	106.27
	B_T	12.40
	R^2	0.727

happened at the biochar-NH_2 surface and includes monolayer coverage formation. Also, from the data considered in Table 4, the theoretical and experimental values of the maximum monolayer coverage (q_m) from the LGR model were very close. The determined maximum sorption capacity from this study was 140.85 mg/g. The sorption capacity of the biochar-NH_2 for Cu(II) ion was high when compared to other biosorbent employed for the confiscation of Cu(II) ion (Table 5).

3.6 Regeneration of biochar-NH_2

Adsorption of pollutants using adsorbent materials is a widely utilized technology for confiscation pollutants from wastewater, and the economics of this technology is highly dependent on the reuse/recycling of these

Table 5 Comparison of the maximum sorption capacity of biochar-NH_2 for Cu(II) confiscation with other adsorbents

Biosorbents	Maximum sorption capacity (mg g^{-1})	References
Biochar-NH_2 synthesized from WWP	140.85	This study
Nanomodified sugarcane bagasse	2.53–2.61	[53]
Banana peel	20.37	[84]
Sawdust	1.79	[85]
Pyrolytic tyre char	0.71	[86]
Watermelon shell	111.10	[71]
Watermelon shell	9.57	[87]
Watermelon rind (*Citrullus lanatus*)	39.20	[88]
Activated watermelon	31.25	[89]
Watermelon shell	111.10	[90]
Thevetia peruviana leaf powder	187.51	[91]

adsorbent materials. The chemical regeneration procedures are used to recharge depleted biochar-NH_2. The biochar-NH_2 was regenerated using 0.10 M of HCl and NaOH followed by rinsing with hot distilled water. After six regeneration cycles, the maximum confiscation of Cu(II) ion by biochar-NH_2 was determined to be 90.23% (Fig. 10b), demonstrating the regeneration capability of biochar-NH_2.

4 Conclusion

The ability of biochar-NH_2 biosorbent synthesized from WMP was explored in the sequestration of Cu(II) in this study. Some parameters such as pH, adsorbent dosage, initial Cu(II) concentration, and contact time were ascertained to impact the effective confiscation of Cu(II) ion using the synthesized biosorbent for this study. The adsorption of Cu(II) to biochar-NH_2 biosorbent was ideally defined employing the LGR and PSO models, and the determined adsorption capacity was 140.85 mg/g which is one of the highest when compared to existing research data in the sequestration of Cu(II) using biosorbents. The study further shows that the biosorbent can be regenerated up to six regeneration cycles. Results from this study show that biosorbent prepared from WMP, which was a low-cost agricultural waste material, can effectively be useful for the confiscation of other heavy metals from WW.

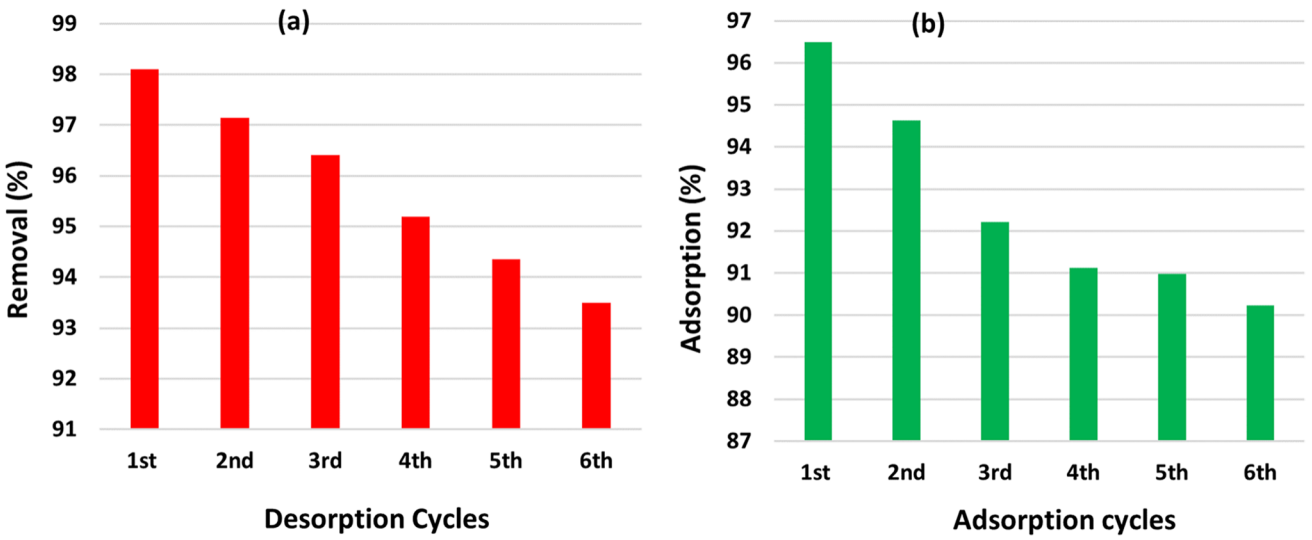

Fig. 10 The influence of regeneration cycles for **a** desorption % of Cu(II) ion from biochar-NH_2, **b** adsorption % of Cu(II) ion on biochar-NH_2 utilizing adsorbent dose (3 g L^{-1}) and Cu(II) ion initial concentration (200 mg L^{-1}) at 25 ± 2 °C

Funding This work was partially funded by the Science and Technology Development Fund (STDF) of Egypt (Projects Nos. CB-4874 and CB-22816).

Data availability Data sharing does not apply to this article.

Declarations

Consent to participate Not applicable.

Conflict of interest The authors declare no competing interests.

References

1. Ukhurebor KE, Athar H, Adetunji CO, Aigbe UO, Onyancha RB, Abifarin O (2021) Environmental implications of petroleum spillages in the Niger Delta region of Nigeria: a review. J Environ Managem 293:112872
2. Onyancha RB, Aigbe UO, Ukhurebor KE, Muchiri PW (2021) Facile synthesis and applications of carbon nanotubes in heavy metal remediation and biomedical fields: a comprehensive review. J Mol Struct 1238:130462
3. Onyancha RB, Ukhurebor KE, Aigbe UO, Osibote OA, Kusuma HS, Darmokoesoemo H, Balogun VA (2021) A systematic review on the detection and monitoring of toxic gases using carbon nanotube-based biosensors. Sens Bio-Sens Res 34:100463
4. Ukhurebor KE, Aigbe UO, Onyancha RB, Nwankwo W, Osibote OA, Paumo HK, Ama OM, Adetunji CO, Siloko IU (2021) Effect of hexavalent chromium on the environment and removal techniques: a review. J Environ Managem 280:111809
5. Aigbe UO, Onyancha RB, Ukhurebor KE, Obodo KO (2020) Removal of fluoride ions using polypyrrole magnetic nanocomposite influenced by rotating magnetic field. RSC Adv 10(1):595–609
6. El Nemr A (2011) Impact, monitoring and management of environmental pollution, Nova Science Publishers, Inc. Hauppauge New York. [ISBN-10: 1608764877, ISBN-13: 9781608764877] 1–638
7. El Nemr A (2012) Environmental pollution and its relation to climate change, Nova Science Publishers, Inc. Hauppauge New York. [ISBN-13: 978–1–61761–794–2] 694 pages
8. Rezania S, Taib SM, Din MFM, Dahalan FA, Kamyab H (2016) Comprehensive review on phytotechnology: heavy metals removal by diverse aquatic plants species from wastewater. J Hazard Mater 318:587–599
9. Sudarni DHA, Aigbe UO, Ukhurebor KE, Onyancha RB, Kusuma HS, Darmokoesoemo H, Osibote OA, Balogun VA, Widyaningrum BA (2021) Malachite green removal by activated potassium hydroxide clove leaves agro-waste biosorbent: characterization, kinetics, isotherms and thermodynamics studies. Adsorp Sci Technol 1145312:1–15
10. Ben-Ali S, Jaouali I, Souissi-Najar S, Ouederni A (2017) Characterization and adsorption capacity of raw pomegranate peel biosorbent for copper removal. J Cleaner Product 142:3809–3821
11. Kerry RG, Ukhurebor KE, Kumari S, Maurya GK, Patra S, Panigrahi B, Majhi S, Rout JR, Rodriguez-Torres MDP, Das G, Shin H-S, Patra JK (2021) A comprehensive review on the applications of nano-biosensor based approaches for non-communicable and communicable disease detection. Biomater Sci 9:3576–3602
12. Ukhurebor KE, Singh KRB, Nayak V, UK-Eghonghon G, (2021) Influence of SARS-CoV-2 pandemic: a review from the climate change perspective. Environ Sci: Proces Impacts 23:1060–1078
13. Ukhurebor KE, Azi SO, Aigbe UO, Onyancha RB, Emegha JO (2020) Analysing the uncertainties between reanalysis meteorological data and ground measured meteorological data. Measurement 165:108110
14. Phuengphai P, Singjanusong T, Kheangkhun N, Amnuay Wattanakornsiri A (2021) Removal of copper (II) from aqueous solution using chemically modified fruit peels as efficient low-cost biosorbents. Water Sci Eng. https://doi.org/10.1016/j.wse.2021.08.003
15. Ukhurebor KE, Aidonojie PA (2021) The influence of climate change on food innovation technology: review on topical developments and legal framework. Agric & Food Secur 10(50):1–14. https://doi.org/10.1186/s40066-021-00327-4
16. Gupta H, Parag R, Gogate PR (2016) Intensified removal of copper from waste water using activated watermelon based biosorbent in the presence of ultrasound. Ultrasonics Sonochem 30:113–122
17. Khaled A, El Nemr A, El Sikaily A (2013) Heavy metals concentrations in biota of the Mediterranean Sea: a review. Part I Blue Biotech J 2(1):79–133
18. Khaled A, El Nemr A, El Sikaily A (2013) Heavy metals concentrations in biota of the Mediterranean Sea: a review, Part II. Blue Biotech J 2(2):191–249
19. Doebrich J, Linda Masonic L (2009) Copper—a metal for the ages. United States Geological Survey, Fact Sheet 2009–3031, May 2009. https://pubs.usgs.gov/fs/2009/3031/FS2009-3031. Accessed 16 Jan 2022
20. El-Sikaily A, El Nemr A, Khaled A (2011) Copper sorption onto dried red alga Pterocladia capillacea and its activated carbon. Chem Eng J 168:707–714
21. El Nemr A, El Sadaawy MM, Khaled A, El Sikaily A (2014) Adsorption of the anionic dye Direct Red 23 onto new activated carbons developed from Cynara cardunculus: kinetics, equilibrium and thermodynamics. Blue Biotech J 3(1):121–142
22. Villen-Guzman M, Gutierrez-Pinilla D, Gomez-Lahoz C, Vereda-Alonso C, Rodriguez-Maroto JM, Arhoun B (2019) Optimization of Ni(II) biosorption from aqueous solution on modified lemon peel. Environ Res 179:108849
23. Ngabura M, Hussain SA, Ghani WAWA, Jami MS, Tan YP (2018) Utilization of renewable durian peels for biosorption of zinc from wastewater. J Environ Chem Eng 6(2):2528–2539
24. Alghamdi MM, El-Zahhar AA, Idris AM, Sadi TO, Sahlabji T, El Nemr A (2019) Synthesis, characterization and application of a new polymeric-clay-magnetite composite resin for water softening. Sep Purif Technol 224:356–365. https://doi.org/10.1016/j.seppur.2019.05.037
25. Chen Q, Yao Y, Li X, Lu J, Zhou J, Huang Z (2018) Comparison of heavy metal removals from aqueous solutions by chemical precipitation and characteristics of precipitates. J Water Process Eng 26:289–300
26. Wu H, Wang W, Huang Y, Han G, Yang S, Su S, Sana H, Peng W, Cao Y, Liu J (2019) Comprehensive evaluation on a prospective precipitation-flotation process for metal-ions removal from wastewater simulants. J Hazard Mater 371:592–602
27. Yesil H, Tugtas AE (2019) Removal of heavy metals from leaching effluents of sewage sludge via supported liquid membranes. Sci Total Environ 693:133608
28. Guyo U, Mhonyera J, Moyo M (2015) Pb(II) adsorption from aqueous solutions by raw and treated biomass of maize stover: a comparative study. Process Safety Environ Protect 93:192–200
29. Khaled A, El Nemr A, El-Sikaily A, Abdelwahab O (2005) Biosorption of basic blue nine from water solution by marine algae. Egypt J Aquat Res 31:130–141

30. Aksu Z, İşoğlu İA (2005) Removal of copper (II) ions from aqueous solution by biosorption onto agricultural waste sugar beet pulp. Process Biochem 40(9):3031–3044
31. El Nemr A, Abdelwahab AO, Khaled A, El-Sikaily A (2005) Removal of chrysophenine from aqueous solution by *Ulva Lactuca*. Egypt J Aquat Res 31:86–98
32. Keawkim K, Khamthip A (2018) Removal of Pb^{2+} ion from industrial wastewater by new efficient biosorbents of Oyster plant (Tradescantia spathacea Steam) and Negkassar leaf (Mammea siamensis T. Anderson). Chiang Mai J Sci 45(1):369–379
33. Sun H, Xia N, Liu Z, Kong F, Wang S (2019) Removal of copper and cadmium ions from alkaline solutions using chitosan-tannin functional paper materials as adsorbent. Chemosphere 236:124370
34. Ismael MN, El Nemr A, El Sayed H, Hamid HA (2020) Removal of hexavalent chromium by cross-linking chitosan and *N*, *N*'-methylene bis-acrylamide. Environ Process 7:911–930. https://doi.org/10.1007/s40710-020-00447-2
35. Hosain AN, El Nemr A, El Sikaily A, Mahmoud ME, Amira MF (2020) Surface modifications of nanochitosan coated magnetic nanoparticles and their applications in Pb(II), Cu(II) and Cd(II) removal. J Environ Chem Eng 8(5):104316. https://doi.org/10.1016/j.jece.2020.104316
36. El Nemr A, El-Assal AA, El Sikaily A, Mahmoud ME, Amira MF, Ragab S (2021) New magnetic cellulose nanobiocomposites for Cu(II), Cd(II) and Pb(II) ions removal: kinetics, thermodynamics and analytical evaluation. Nanotech Environ Eng 6(3):1–20. https://doi.org/10.1007/s41204-021-00138-9
37. Manzoor Q, Nadeem R, Iqbal M, Saeed R, Ansari TM (2013) Organic acids pretreatment effect on Rosa bourbonia phytobiomass for removal of Pb(II) and Cu (II) from aqueous media. Bioresour Technol 132:446–452
38. Tasaso P (2014) Adsorption of copper using pomelo peel and depectinated pomelo peel. J Clean Energy Tech 2(2):154–157
39. Romero-Cano LA, García-Rosero H, Gonzalez-Gutierrez LV, Baldenegro-Pérez LA, Carrasco-Marín F (2017) Functionalized adsorbents prepared from fruit peels: equilibrium, kinetic and thermodynamic studies for copper adsorption in aqueous solution. J Cleaner Prod 162:195–204
40. Safari E, Rahemi N, Kahforoushan D, Allahyari S (2019) Copper adsorptive removal from aqueous solution by orange peel residue carbon nanoparticles synthesized by combustion method using response surface methodology. J Environ Chem Eng 7(1):102847
41. Semercioöz AS, Göğüş F, Çelekli A, Bozkurt H (2017) Development of carbonaceous material from grapefruit peel with microwave implemented-low temperature hydrothermal carbonization technique for the adsorption of Cu(II). J Cleaner Prod 165:599–610
42. Zhang W, Song J, He Q, Wang H, Lyu W, Feng H, Xiong W, Guo W, Wu J, Chen L (2020) Novel pectin based composite hydrogel derived from grapefruit peel for enhanced Cu(II) removal. J Hazard Mater 384:121445
43. El-Nemr MA, Abdelmonem NM, Ismail IM, Ragab S, El Nemr A (2020) Ozone and ammonium hydroxide modification of biochar prepared from *Pisum sativum* peels improves the adsorption of copper (II) from an aqueous medium. Environ Process 7(3):973–1007. https://doi.org/10.1007/s40710-020-00455-2
44. Eldeeb TM, El Nemr A, Khedr MH, El-Dek SI (2021) Efficient removal of Cu(II) from water solution using magnetic chitosan nanocomposite. Nanotechnol Environ Eng 6(2):1–15. https://doi.org/10.1007/s41204-021-00129-w
45. Eldeeb TM, El-Nemr A, Khedr MH, El-Dek SI (2021) Novel bionanocomposite for efficient copper removal. Egypt J Aquat Res 47(3):261–267. https://doi.org/10.1016/j.ejar.2021.07.002
46. Gregg SJ, Sing KSW (1982) Adsorption surface area and porosity, 2nd edn. Academic Press INC., London, pp 957–957
47. Rouquerol F, Rouquerol J, Sing KSW (1999) Adsorption by powders and porous solids. Academic Press INC., London
48. Barrett EP, Joyner LG, Halenda PP (1951) The determination of pore volume and area distributions in porous substances. I. Computations from nitrogen isotherms. J Amer Chem Soc 73(1):373–380
49. El-Nemr MA, Abdelmonem NM, Ismail IMA, Ragab S, El Nemr A (2020) Removal of acid yellow 11 dye using novel modified biochar derived from watermelon peels. Desal Water Treat 203:403–431
50. El-Nemr MA, Ismail IMA, Abdelmonem NM, El Nemr A, Ragab S (2021) Amination of biochar derived from watermelon peel by triethylenetetramine and ammonium hydroxide for toxic chromium removal enhancement. Chin J Chem Eng 36:199–222
51. Duan C, Ma T, Wang J, Zhou Y (2020) Removal of heavy metals from aqueous solution using carbon-based adsorbents: a review. J Water Process Eng 37:101339
52. El Nemr A, Shoaib AGM, El Sikaily A, Ragab S, Mohamed AE-DA, Hassan AF (2021) Utilization of green alga *Ulva lactuca* for sustainable production of meso-micro porous nano activated carbon for adsorption of direct red 23 dye from aquatic environment. Carb Lett. https://doi.org/10.1007/s42823-021-00262-1 (In press)
53. Carvalho JTT, Milani PA, Consonni JL, Labuto G, Carrilho ENVM (2021) Nanomodified sugarcane bagasse biosorbent: synthesis, characterization, and application for Cu (II) removal from aqueous medium. Environ Sci Poll Res 28(19):24744–24755
54. Shoaib AG, El-Sikaily A, El Nemr A, Mohamed AEDA, Hassan AA (2020) Preparation and characterization of highly surface area activated carbons followed type IV from marine red alga (Pterocladia capillacea) by zinc chloride activation. Biomass Conv Bioref. https://doi.org/10.1007/s13399-020-00760-8 (in press)
55. Shoaib AG, El-Sikaily A, El Nemr A, Mohamed AEDA, Hassan AA (2020) Testing the carbonization condition for high surface area preparation of activated carbon followed type IV from green alga *Ulva Lactuca*. Biomass Conv Bioref. https://doi.org/10.1007/s13399-020-00823-w (in press)
56. Aigbe UO, Osibote OA (2021) Carbon derived nanomaterials for the sorption of heavy metals from aqueous solution: a review. Environ Nanotechnol Monitor Manag 16:100578
57. Arslanoğlu H, Kaya S, Tümen F (2020) Cr (VI) adsorption on low-cost activated carbon developed from grape marc-vinasse mixture. Particul Sci Technol 38(6):768–781
58. Aigbe UO, Osibote OA (2020) A review of hexavalent chromium removal from aqueous solutions by sorption technique using nanomaterials. J Environ Chem Eng 8:104503
59. Eleryan A, El Nemr A, Idris AM, Alghamdi MM, El-Zahhar AA, Said TO, Sahlabji T (2020) Feasible and eco-friendly removal of hexavalent chromium toxicant from aqueous solutions using chemically modified sugarcane bagasse cellulose. Toxin Rev. https://doi.org/10.1080/15569543.2020.1790606 (in press)
60. El Nemr A, Aboughaly RM, El Sikaily A, Ragab S, Masoud MS, Ramadan MS (2020) Microporous nano activated carbon type I derived from orange peel and its application for Cr(VI) removal from aquatic environment. Biomass Conv Bioref. https://doi.org/10.1007/s13399-020-00995-5 (in press)
61. El Nemr A, Aboughaly RM, El Sikaily A, Ragab S, Masoud MS, Ramadan MS (2021) Utilization of sugarcane bagasse/$ZnCl_2$ for sustainable production of microporous nano activated carbons of type I for toxic Cr(VI) removal from aqueous environment. Biomass Conv Bioref. https://doi.org/10.1007/s13399-021-01445-6
62. Mohamad OA, Hao X, Xie P, Hatab S, Lin Y, Wei G (2009) Biosorption of copper (II) from aqueous solution using non-living

mesorhizobium amorphae strain CCNWGS0123. Microbes Environ 27(3):234–241. https://doi.org/10.1264/jsme2.ME11331
63. Sahlabji T, El-Nemr MA, El Nemr A, Ragab S, Alghamdi MM, El-Zahhar AA, Idris AM, Said TO (2021) High surface area microporous activated carbon from *Pisum sativum* peels for hexavalent chromium removal from aquatic environment. Toxin Rev. https://doi.org/10.1080/15569543.2021.1908361 (in press)
64. Wang G, Zhang S, Yao P, Chen Y, Xu X, Li T, Gong G (2018) Removal of Pb (II) from aqueous solutions by Phytolacca americana L. biomass as a low cost biosorbent. Arab J Chem 11(1):99–110
65. Ismail MNM, El Nemr A, El Ashry ESH, Abdel Hamid H (2020) Novel simple modification of chitosan as adsorptive agent for removal of Cr^{6+} from aqueous solution. Egypt J Chem 63(4):1219–1240. https://doi.org/10.21608/ejchem.2019.11157.1716
66. Duan C, Ma T, Wang J, Zhou Y (2020) Removal of heavy metals from aqueous solution using carbon-based adsorbents: a review. J Water Process Eng 37:101339
67. Mohammed TJ, Ibrahim RI (2016) Remediation of Cu (II) from well water of Iraq by using cortex of fruits and agricultural waste. Arab J Sci Eng 41(2):345–355
68. Foroutan R, Peighambardoust SJ, Peighambardoust SH, Pateiro M, Lorenzo JM (2021) Adsorption of crystal violet dye using activated carbon of lemon wood and activated carbon/Fe_3O_4 magnetic nanocomposite from aqueous solutions: a kinetic, equilibrium and thermodynamic study. Molecules 26(8):2241
69. Benzaoui T, Selatnia A, Djabali D (2018) Adsorption of copper (II) ions from aqueous solution using bottom ash of expired drugs incineration. Adsorpt Sci Technol 36(1–2):114–129
70. El Nemr A, El-Sikaily A, Khaled A (2010) Modeling of adsorption isotherms of methylene blue onto rice husk activated carbon. Egypt J Aquat Res 36(3):403–425
71. Banerjee K, Ramesh ST, Gandhimathi R, Nidheesh PV, Bharathi KS (2012) A novel agricultural waste adsorbent, watermelon shell for the removal of copper from aqueous solutions. Iranica J Ener Environ 3(2):143–156
72. Hassaan MA, El Nemr A, Madkour FF (2017) Testing the advanced oxidation processes on the degradation of direct blue 86 dye in wastewater. Egypt J Aquat Res 43:11–19. https://doi.org/10.1016/j.ejar.2016.09.006
73. Hassaan MA, El Nemr A, Madkour FF (2017) Advanced oxidation processes of mordant violet 40 dye in freshwater and seawater. Egypt J Aquat Res 43(1):1–9. https://doi.org/10.1016/j.ejar.2016.09.004
74. Grover A, Mohiuddin I, Malik AK, Aulakh JS, Vikrant K, Kim KH, Brown RJ (2021) Magnesium/aluminum layered double hydroxides intercalated with starch for effective adsorptive removal of anionic dyes. J Hazard Mater 424:127454
75. Adebayo GB, Jamiu W, Okoro HK, Okeola FO, Adesina AK, Feyisetan OA (2019) Kinetics, thermodynamics and isothermal modelling of liquid phase adsorption of methylene blue onto moringa pod husk activated carbon. South Afr J Chem 72:263–237
76. Fernandes T, Soares SF, Trindade T, Daniel-da-Silva AL (2017) Magnetic hybrid nanosorbents for the uptake of paraquat from water. Nanomaterials 7(3):68
77. Jadhav AS, Mohanraj GT (2017) Evaluation of kinetic models of lead uptake from wastewater by activated carbon derived from coconut leaves. Nature Environ Pollut Technol 6(1):189–197
78. López-Luna J, Ramírez-Montes LE, Martinez-Vargas S, Martínez AI, Mijangos-Ricardez OF, María del Carmen A, Carrillo-González R, Solís-Domínguez FA, del Carmen C-Díaz M, Vázquez-Hipólito V (2019) Linear and nonlinear kinetic and isotherm adsorption models for arsenic removal by manganese ferrite nanoparticles. SN Appl Sci 1(8):1–19
79. Ofomaja AE, Naidoo EB, Pholosi A (2020) Intraparticle diffusion of Cr (VI) through biomass and magnetite coated biomass: a comparative kinetic and diffusion study. South Afr J Chem Eng 32(1):39–55
80. Cao Q, Huang Z, Liu S, Wu Y (2019) Potential of Punica granatum biochar to adsorb Cu (II) in soil. Sci Rep 9(1):1–13
81. Taib NI, Rosli NA, Saharrudin NI, Rozi NM, Kasdiehram NAA, Abu Nazri NNT (2021) Kinetic, equilibrium, and thermodynamic studies of untreated watermelon peels for removal of copper (II) from aqueous solution. Desal Water Treat 227:289–299
82 Lucaci AR, Bulgariu D, Ahmad I, Bulgariu L (2020) Equilibrium and kinetics studies of metal ions biosorption on alginate extracted from marine red algae biomass (Callithamnion corymbosum sp.). Polymers 12(9):1888
83. Ayawei N, Ebelegi AN, Wankasi D (2017) Modelling and interpretation of adsorption isotherms. J Chem 2017:3039817. https://doi.org/10.1155/2017/3039817
84. Hossain MA, Ngo HH, Guo WS, Nguyen TV (2012) Biosorption of Cu (II) from water by banana peel based biosorbent: experiments and models of adsorption and desorption. J Water Sustain 2(1):87–104
85. Bin Yu YZ, Shukla A, Shukla SS, Dorris KL (2001) The removal of heavy metals from aqueous solutions by sawdust adsorption—removal of lead and comparison of its adsorption with copper. J Hazard Mater B 84:83–94
86. Shahtalebi A, Sarrafzadeh MH, McKay G (2013) An adsorption diffusion model for removal of copper (II) from aqueous solution by pyrolytic tyre char. Desal Water Treat 51(28–30):5664–5673
87. Ibrahim RI (2020) Optimization process for removing of copper ions from groundwater of Iraq using watermelon shells as natural adsorbent. IOP Conf Ser Mater Sci Eng 737(1):012195
88. Lakshmipathy R, Sarada NC (2016) Metal ion free watermelon (Citrullus lanatus) rind as adsorbent for the removal of lead and copper ions from aqueous solution. Desalin Water Treat 57(33):15362–15372
89. Gupta H, Gogate PR (2016) Intensified removal of copper from waste water using activated watermelon based biosorbent in the presence of ultrasound. Ultrason Sonochem 30:113–122
90. Banerjee K, Ramesh ST, Gandhimathi R, Nidheesh PV, Bharathi KS (2012) A novel agricultural waste adsorbent, watermelon shell for the removal of copper from aqueous solutions. Iran J Energy Environ 3(2):143–156
91. Medhi H, Chowdhury PR, Baruah PD, Bhattacharyya KG (2020) Kinetics of aqueous Cu (II) biosorption onto Thevetia peruviana leaf powder. ACS Omega 5(23):13489–13502